Performance evaluations and applications of a δ^{13}C-DIC analyzer in seawater and estuarine waters

Xue Deng[1,2,3], Qian Li[1], Jianzhong Su[1,4], Chun-Ying Liu[2], Eliot Atekwana[5], Wei-Jun Cai[1,*]

[1] School of Marine Science and Policy, University of Delaware, Newark, DE, 19716, USA

[2]Frontiers Science Center for Deep Ocean Multispheres and Earth System, Key Laboratory of Marine Chemistry Theory and Technology, Ministry of Education, College of Chemistry and Chemical Engineering, Ocean University of China, Qingdao 266100, PR China

[3]Key Laboratory for Ecological Environment in Coastal Areas (State Oceanic Administration), National Marine Environmental Monitoring Center, Dalian 116023, China

[4]State Key Laboratory of Marine Resources Utilization in South China Sea, Hainan University, Haikou, 570228, China

[5] Earth and Planetary Sciences Department, University of California Davis, Davis, CA 95616 USA

***Corresponding author: wcai@udel.edu**

Abstract:

Dissolved inorganic carbon (DIC) and its stable isotope (δ^{13}C-DIC) are important parameters for studying carbon cycling in aquatic environments. Traditional methods based on isotope-ratio mass spectrometers are labor-intensive and not easily deployable at field sites. Here we report the performance of a method that simultaneously measures DIC concentration and its stable isotope by using a CO_2 extraction device and a Cavity Ring-Down Spectroscopy (CRDS) detector. A multi-port valve is used to increase sample throughput and improve precision. The instrument achieves average precisions of better than ± 1.95 μmol kg^{-1} and ± 0.06‰, respectively, for DIC and δ^{13}C-DIC in seawater based on three injections for each sample. We also provide recommendations on how to precisely determine δ^{13}C-DIC samples with a wide range of DIC content in different types of waters by examining injection volume and concentration effects. This technique was applied to study carbon cycling in the Delaware Estuary. It demonstrates that a combined determination of both DIC and δ^{13}C-DIC is a powerful tool for constraining the processes controlling aquatic carbon cycling and CO_2 fluxes. Both laboratory tests and field applications confirmed that this system can be used with high precision to study carbon cycling in various aquatic environments.

Keywords: Dissolved inorganic carbon; Stable carbon isotope δ^{13}C-DIC; Cavity Ring-Down Spectroscopy; Continuous measurement; Delaware Estuary

Running head: Laboratory and field assessments of a δ^{13}C-DIC analyzer

Synopsis: This analyzer provides a precise, rapid, and onsite analysis of inorganic carbon concentration and its stable isotope (δ^{13}C-DIC) in aquatic environments.

Highlights

- Instrument and technique to simultaneously and precisely measure DIC concertation and δ^{13}C-DIC
- Instrument is portable and can be deployed at field sites and onboard ships
- Recommendations on how to precisely determine δ^{13}C-DIC samples with different DIC contents
- The system will enhance spatiotemporal near real-time analysis of DIC and δ^{13}C-DIC

Graphic Abstract

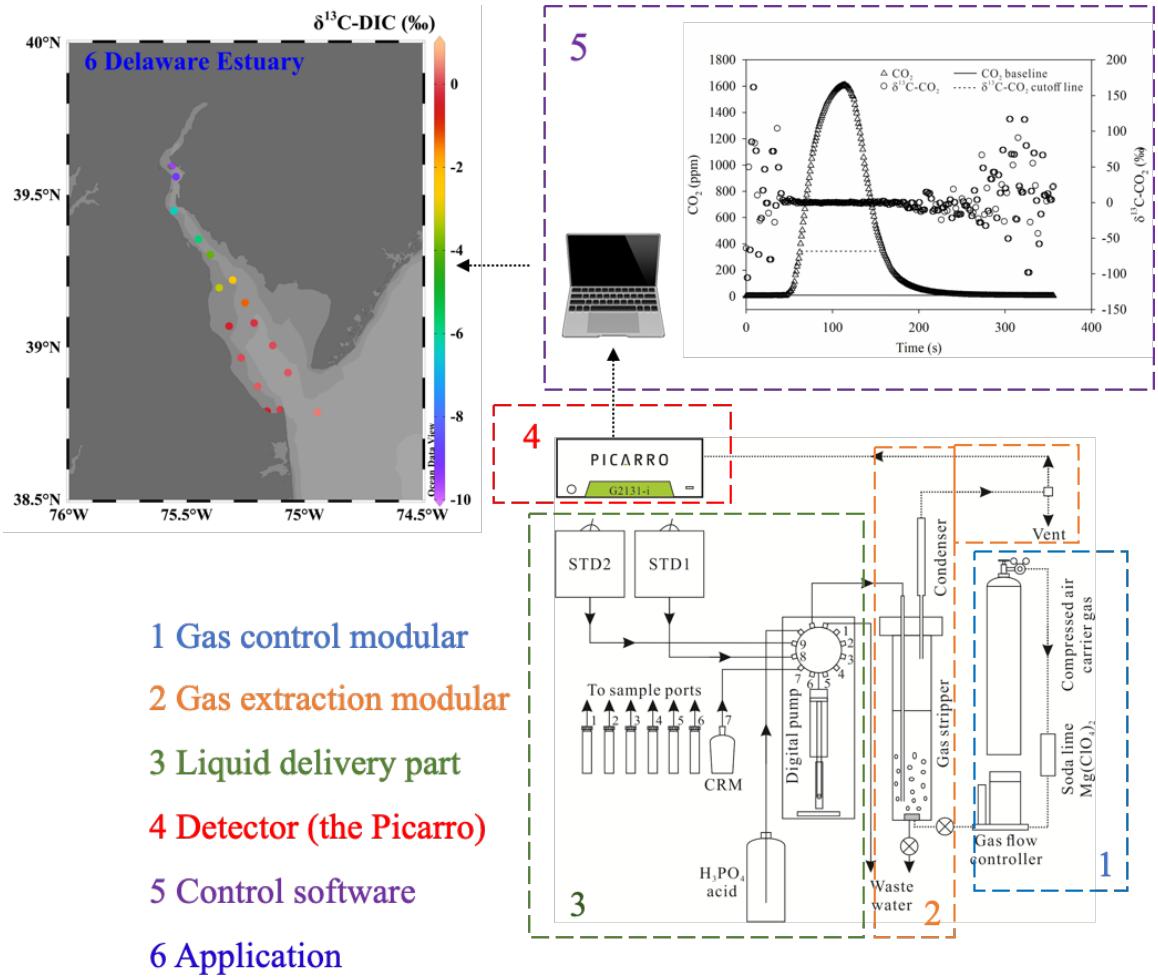

1 Introduction

Dissolved inorganic carbon (DIC) is the primary carbon pool in natural waters and its quantification is essential for studying the global carbon cycle. The stable isotope of DIC (δ^{13}C-DIC) is a powerful tool for determining the sources and sinks of DIC and in understanding carbon cycling and the associated biogeochemical processes in aquatic ecosystems[1–8]. In particular, the δ^{13}C-DIC can be used to elucidate whether the source of DIC is allochthonous or autochthonous and can be used to separate the relative contributions among different pools of organic matter degradation, biological production, and physical processes that control DIC dynamics in the ocean and coastal waters[1,3,9,10]. In addition, the δ^{13}C-DIC is a useful tracer in determining anthropogenic CO_2 uptake rate by the ocean and can be used to identify whether an ocean region is a sink for anthropogenic CO_2[11,12].

In most oceanographic and hydrogeological studies, the δ^{13}C-DIC is measured by gas source isotope-ratio mass spectrometry (IRMS). The high precision and accuracy have made IRMS the preferred conventional technique for determining δ^{13}C-DIC over the last several decades[13–17]. However, the disadvantages of the IRMS-based conventional technique (e.g., the high level of required expertise for sample pretreatment and analysis, the complexity of equipment set-up, the expensive instrument maintenance, the inability to deploy in the field) limit the ability to conduct δ^{13}C-DIC studies with high temporal and spatial resolutions[18,19]. In open ocean transect cruises, water samples were collected,

71 preserved and usually transported back to land-based laboratories for δ^{13}C-DIC analysis by
72 the IRMS technique. Thus, compared to the direct DIC concentration analysis onboard for
73 every sampling station and depth, only <15% of samples have corresponding δ^{13}C-DIC
74 analysis[20]. Therefore, lower spatial and temporal δ^{13}C-DIC coverages limit the full benefits
75 of the δ^{13}C-DIC as a more sensitive tracer than DIC for the study of anthropogenic CO_2
76 uptake and biogeochemical processes[11,12]. Finally, a lack of the flexibility of making
77 immediate decisions on issues such as adding additional sampling stations and times based
78 on feedbacks from onsite analysis is another obvious disadvantage of the use of the
79 traditional IRMS method.

80 In recent years, extensive efforts have been made to overcome the limitations of the
81 IRMS-based conventional technique, especially automation of sample preparation and
82 deployability to conduct near-real-time δ^{13}C-DIC analysis. Among these, the laser-based
83 optical spectroscopy has gained increasing recognition and is a suitable alternative
84 approach to simultaneously measure DIC concentrations and δ^{13}C-DIC values because of
85 its high detection sensitivity, relatively straightforward experimental set-up, and field-
86 portability[6,21–25]. For example, Bass et al.[21] utilized a continuous, automated DIC analyzer
87 to monitor DIC concentrations and its δ^{13}C-DIC signals in water samples. However, their
88 method required large sample volumes (350 mL) and their precision of ± 10 μmol kg^{-1} for
89 DIC and ± 0.2‰ for δ^{13}C-DIC is inadequate for studying DIC processes with small
90 variations or slow rates. Call et al.[22] coupled a commercially available non-dispersive

91 infrared (NDIR) CO_2 detector based DIC analyzer to a Cavity Ring-Down Spectroscopy
92 (CRDS) isotope analyzer to determine DIC concentrations and δ^{13}C-DIC values,
93 respectively, with high precisions of ± 1.5–2.0 μmol kg^{-1} for DIC and ± 0.14‰ for the
94 δ^{13}C-DIC, when DIC concentrations ranged from 1000 to 3600 μmol kg^{-1}. In the approach,
95 the NDIR detector was used to measure DIC with one injection of the sample while the
96 CRDS detector was used to measure δ^{13}C-DIC with different injection, and the two
97 injections had different analytical conditions (i.e., the gas flow rate was 300 mL min^{-1} in
98 the former and 70 mL min^{-1} in the latter). The fact that this approach requires two detectors
99 and two different analytical procedures for DIC and δ^{13}C-DIC probably has limited its
100 application.

101 As an improvement, Su et al.[6] used one CRDS detector and a single procedure to
102 simultaneously quantify both DIC and δ^{13}C-DIC. In this approach, 3–4 mL samples were
103 acidified to transfer DIC to CO_2 and then both DIC concentration and its carbon isotope
104 ratio were determined by the Picarro G2131-i CRDS analyzer to achieve precisions of ±
105 1.5 μmol kg^{-1} for DIC and ± 0.09‰ for δ^{13}C-DIC. However, in both Call et al.[22] and Su et
106 al.[6] methods, once a sample analysis is completed, an operator needs to manually load
107 another sample, which is still labor-intensive and limits the sample throughput rate. The
108 approaches may also limit the analytical precision due to less consistency between analyses
109 (e.g., time interval between samples varies). Therefore, though initial results were

published in Su et al.[6], further automation, improvements, and extensive evaluations of the performance of the analytical techniques and system are highly needed.

In the present study, we improved the instrument's sampling procedure from a single sample valve in Su et al.[6] to a multi-port valve to achieve automated multi-sample analysis with less labor-intensive monitoring and operation. The use of the multi-port valve is also expected to provide a better consistency among different samples and thus to improve the overall analytical precision. We have carried out both extensive laboratory tests and field sample analysis to evaluate the performance of the upgraded method and system. First, we examined the repeatability of the multi-port valve to ensure that all sample channels are identical in sample delivery and work consistently. Because we drew samples from the same stock of seawater, this experiment provided a rigorous evaluation of the analytical precision and the analytical system stability. Furthermore, the sample injection volume and DIC concentration experiments were conducted to determine the injection volume range for δ^{13}C-DIC samples with different DIC concentrations in different types of aquatic environments. Finally, we demonstrated the applicability and advantages of this new CRDS-based method via a comprehensive field study of the carbonate system in the Delaware Estuary.

2 Materials and Methods

2.1 Instrument structure and principle

A whole-water CO_2 extraction device with a 12-port sample valve (AS-D1, Apollo Scitech, Newark, DE, USA; www.apolloscitech.com) and a CRDS isotopic detector (G2131-i, Picarro, Santa Clara, CA, USA www.picarro.com), were coupled and automated with a single software to simultaneously measure DIC concentrations and δ^{13}C-DIC signals via quantifying the CO_2 extracted from acidified samples (Fig. 1). The principle of a previous version of this system was described in Su et al.[6] and the AS-D1 device specifics and procedures of sample analysis have been introduced in Cheng et al.[26]. Briefly, an aliquot of sample is acidified with 5% H_3PO_4 in the gas stripping reactor and the liberated CO_2 is brought by the carrier gas (CO_2-free compressed air) to the CRDS analyzer, where DIC concentration and δ^{13}C-DIC signal are determined simultaneously. The CO_2 stripper is composed of a porous bubbler, which is fixed at the bottom of the reactor. The carrier gas bubbles through the sample from the bottom to the top, and carries the liberated CO_2 through a condenser, which condenses the water vapor and minimizes the water vapor correction of the Picarro detector. The outlet pressure of the carrier gas is set to 15 psi, and a gas flow controller is used to precisely control the carrier gas flow rate at 60 mL min^{-1}, which is higher than the input flow rate of the Picarro analyzer (~ 30 mL min^{-1}), to ensure that all the measured CO_2 is CO_2 stripped out from the sample. Thus, about half of the gas stream is released to the room and no pressure is built up at the Picarro inlet side.

We improved the method described by Su et al.[6] by including a 12-port sample valve: one port for acid, another for the injection of sample and acid into the reactor, and a third port for waste, then nine other ports can be used for sample and standard analysis (Fig. 1). One of the sample ports is designated for the DIC standard, such as using a Certified Reference Material (CRM) or another secondary house standard to create a working standard curve for DIC calibration. We also prepared two home-made isotope standards. STD1 (-2.70‰) and STD2 (-19.57‰) were made by dissolving $NaHCO_3$ solids in deionized water, and along with CRM are used to calibrate the δ^{13}C-DIC data. The δ^{13}C-DIC values of the home-made isotope standards and CRM solution were verified by the IRMS technique in the stable isotope facility, University of California, Davis. In an environment with narrow ranges of DIC concentration and δ^{13}C-DIC such as that in seawater (1800—2300 μmol kg^{-1} in DIC and -3 to 2‰ in δ^{13}C-DIC), a single pre-calibrated standard may be enough to serve as both concentration and isotope standard. However, in other environments such as in an estuary, two or even three standards for δ^{13}C-DIC may be desirable.

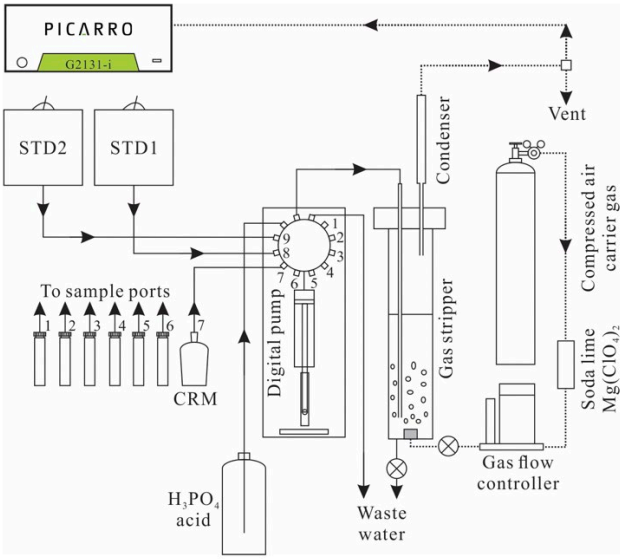

Fig. 1 A schematic layout of the CO_2 extraction device (AS-D1) and CRDS isotope detector (G2131-i) to measure DIC concentrations and $\delta^{13}C$-DIC signals autonomously and simultaneously. A 5-mL syringe is used in this work (note that the syringe volume can be changed to 10 mL for need). For the 12 ports valve, one connects to the acid, one delivers the syringe's liquid to the gas stripper, one discharges to waste, the ports of #1 to #6 are connected to the sample lines and the rest of three ports (#7, #8 and #9) are connected to three standards (CRM, STD1 and STD2), respectively. Port #7 can be run in one single volume or three different volumes of CRM standard for DIC calibration.

As described in Su et al.[6], the area under the curve of the mole fraction CO_2 gas was integrated over time to derive a net area for quantifying DIC concentrations (also included in the upper right corner in the graphic abstract). In this work, three volumes of a CRM or a home-made standard, e.g., 3.0, 3.5 and 4.0 mL, are used to create a working standard

curve between the net area and DIC mole amounts. The latter is calculated as the product of the CRM or home-made standard's volume and known concentration. The DIC concentration of a sample is then derived from the working standard curve and the known injection sample volume.

The δ^{13}C-DIC is derived as the CO_2 weighted mean of δ^{13}C-CO_2 data. Similar to the practice in Su et al.[6] and Call et al.[22], we set a cutoff value to exclude δ^{13}C-CO_2 at low CO_2 concentrations. This is because the Picarro instrument internally determines δ^{13}C-CO_2 by referencing the ^{13}C signal to ^{12}C signal, and thus, at a very low ^{12}C signal, the δ^{13}C-CO_2 signal has high noise and should not be used. A CO_2 range of 380–2000 ppm (or 1000–2000 ppm) is recommended by the manufacturer for a guaranteed isotope analysis precision of 0.1‰ (or 0.05‰) for the Picarro G2131-i. Noted that the cutoff value can be defined by users, for example, 350 ppm was set as the cutoff value in this study. As we adopted a weighted-mean method in our study, the final δ^{13}C-DIC value is not particularly sensitive to the chosen cutoff value, because the noisy δ^{13}C-CO_2 data at low CO_2 only accounts for a small fraction of the entire dataset.

2.2 Preparation of the stock seawater

The stock seawater used in all laboratory experiments was collected from the Gulf of Mexico (GoM) and had been stored in a large tank designed for research supply in the Louisiana Universities Marine Consortium (LUMCON). The seawater was filtered through 0.45 μm cartridge filter and then transferred into a 4 L gastight bag (Cali-5-Bond,

Calibrated Instruments Inc.) and doped with 1 mL $HgCl_2$ to inhibit further biological activities, which is a standard operation protocol for preserving DIC samples[27]. Before preservation, biological respiration likely had increased DIC and decreased δ^{13}C-DIC of this stock water compared to initial values from the GoM surface waters (0.5–1.0‰; Cai's laboratory unpublished data).

2.3 Multi-port valve test, injection volume effect and concentration effect experiments

There is the possibility for cross-contamination caused by sample carryover between subsequent ports when using a multiport valve. Therefore, we assessed if the new multi-port system delivers identical DIC concentrations and δ^{13}C-DIC values between ports. All sample and standard ports in the injection volume of 3.5 mL were connected to the same batch of stock seawater (preparation details in section 2.2) with three consecutive injections per port to assess the multi-port valve injection consistency.

Different aquatic samples from seawater to estuarine, river and lake waters may post different challenges in sample volumes and concentration ranges. To determine if different injection volumes with the same DIC concentration or different DIC concentrations with the same injection volume could affect the measurements of DIC concentrations and δ^{13}C-DIC signals using the CRDS system, we conducted the following experiments. For the injection volume effect experiment, the stock seawater in the same bag was measured in different injection volumes in a sequence from 1.2–5.8 mL at 0.2 mL increment. For the

concentration effect experiment, stock seawater was diluted with CO_2-free deionized water to make a series of solutions with 7 different DIC nominal concentrations, ranging from 250 to 2300 μmol kg^{-1}, then samples were run in the same injection volume (3.5 mL), simulating waters with a wide range of DIC concentration from natural environments.

2.4 Field work in the Delaware Estuary

We evaluated the analytical method and demonstrated its applicability in the Delaware Estuary, which is composed of 100 km long tidal Delaware River and Delaware Bay[28] and has a DIC range of ~1000 μmol kg^{-1} at the river end and ~2000 μmol kg^{-1} at the ocean end. A one-day cruise in the Delaware Estuary was conducted on April 3, 2019 (Fig. 2). The δ^{13}C-DIC and ancillary parameters of surface water were collected along the longitudinal axis in the main channel and the western shoal of the Delaware Estuary to domonstrate the applicability of our DIC and δ^{13}C-DIC analysis method.

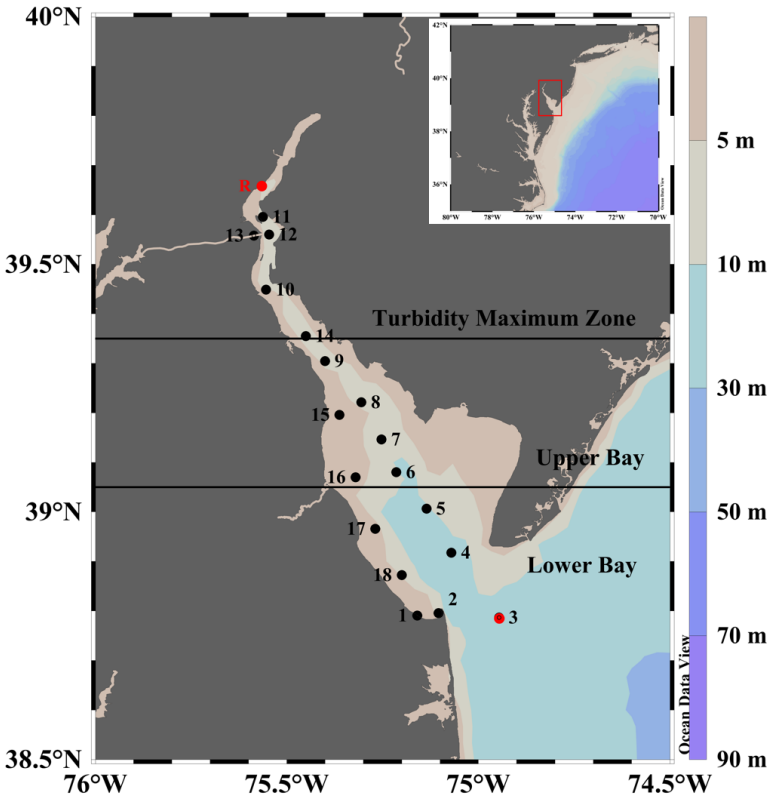

227

228 **Fig. 2** Sampling stations in the Delaware Estuary. The red filled dots represent the river

229 endmember (station R) and ocean endmember (station 3). Delaware Estuary is divided into

230 3 parts (turbidity maximum zone, upper bay and lower bay) by the solid horizontal lines

231 based on Sharp et al.[29]. The inserted regional map represents the location of the Delaware

232 Bay on the US east coast.

233 The DIC and δ^{13}C-DIC samples were determined by the AS-D1 δ^{13}C-DIC analyzer as

234 described above. TA samples were measured by Gran titration with AS-ALK2 (Apollo

235 Scitech) with precision of 0.1%[30], and pH with a Ross combination electrode calibrated

236 against three NBS buffers at 25 ± 0.1°C with a precision of ± 0.005 pH. The partial pressure

237 of CO_2 (pCO_2) was monitored by an underway pCO_2 analyzer (AS-P2, Apollo Scitech)

238 installed in the shipboard laboratory and calibrated against three standard gases[31]. Ca^{2+}
239 samples were measured using a modified technique of Kanamori and Ikegami[32] with a
240 precision <0.1%. Aragonite saturation state (Ω_{Ar}) was derived by using the measured Ca^{2+},
241 calculated CO_3^{2-} and aragonite solubility, according to Mucci[33].

242 **2.5 Two endmember mixing calculation**

243 The DIC concentrations and δ^{13}C-DIC signatures in the Delaware Estuary vary due to
244 several processes including mixing, gas exchange, carbonate precipitation/dissolution and
245 biological processes. Thus, a two-endmember mixing model is used to separate physical
246 mixing effect from other processes. The mixing fractions between two endmembers, river
247 water and seawater, for each sample can be quantified using salinity as a conservative
248 tracer[34,35]:

249 $$f_r + f_{sw} = 1 \quad (1)$$

250 $$S_r \times f_r + S_{sw} \times f_{sw} = S_{meas} \quad (2)$$

251 $$TA_{mix} = TA_r \times f_r + TA_{sw} \times f_{sw} \quad (3)$$

252 $$DIC_{mix} = DIC_r \times f_r + DIC_{sw} \times f_{sw} \quad (4)$$

253 $$DIC_{mix} \times \delta^{13}C\text{-}DIC_{mix} = \delta^{13}C\text{-}DIC_r \times DIC_r \times f_r + \delta^{13}C\text{-}DIC_{sw} \times DIC_{sw} \times f_{sw} \quad (5)$$

254 where f is mixing fraction; the subscripts *r*, *sw*, *mix* and *meas* represent the river end-
255 member, seawater end-member, conservative mixing value and the measured value of
256 sample. Equations (3)–(5) are used to calculate the conservative TA, DIC and δ^{13}C-DIC
257 mixing lines in the two-endmember mixing model. The conservative pH mixing line (at

25°C) is calculated from the conservative DIC and TA with the CO2SYS program[36]. The station R (Fig. 2) in the Delaware River was chosen as the river endmember, since it has near-zero salinity, is minimally affected by tidal movement in spring, and is easily accessible from a pier; Station 3 is located outside the bay mouth and connected with the Atlantic Ocean, thus, is selected as the ocean end-member (Table 1).

Table 1. Summary information of the end-member stations in the two end-member model.

Endmembers	Latitude	Longitude	Salinity	DIC (μmol kg^{-1})	TA (μmol kg^{-1})	δ^{13}C-DIC (‰)
Riverine	39.5800°N	75.5869°W	0.16	970.6 ± 0.6	944.6 ± 0.0	-9.06 ± 0.07
Oceanic	38.7868°N	74.9459°W	30.54	1975.0 ± 0.6	2150.5 ± 1.9	0.37 ± 0.08

3 Results and Discussion

3.1 Analytical precision and repeatability of the multi-port valve

For the same seawater measurements in the nine ports, we obtained a total of 81 raw data in three rounds with three consecutive injections per port. Based on all 81 raw data without any drift correction, the precisions of DIC concentrations and δ^{13}C-DIC values were 1.95 μmol kg^{-1} and 0.06‰ (Fig. 3). These precisions may be viewed as the upper boundary of the method uncertainties, which are slightly better than or similar to the overall analytical precisions of DIC measurements from the traditional NDIR method (0.1%)[30] and δ^{13}C-DIC from the single-port version of this system (0.09‰)[6]. These results indicate that the DIC concentrations and δ^{13}C-DIC values from all ports are not significantly different

from each other, which is also verified by the statistics analysis (ANOVA test, DIC: p = 0.99, n = 81; δ^{13}C-DIC: p = 0.35, n = 81). However, if we first averaged the three consecutive injections on each port and then applied statistical analysis to each round (that is, n = 9 for each round), the deviations were much reduced. The standard deviations of DIC and δ^{13}C-DIC between multi-port valves were 0.9—1.2 μmol kg^{-1} and 0.02—0.04‰, respectively (Table 2 and Fig. 3). Since during our analysis of standards and samples, we made three injections and then use the average of the three injections as the raw data for each standard or sample, the statistical analysis based on the 3-injection averaged data may reflect the true instrument performance better than those based on the individual 81 raw data. We argue that the average of 3-injection based statistics at least point to the potential precision and possibly accuracy this method can achieve if a suitable standardization method can be accomplished in the future. Since the ultimate performance of the instrument is also limited by the calibration and standards, for now, we are content with reporting the precision and accuracy as better than 1.95 μmol kg^{-1} for DIC and 0.06‰ for δ^{13}C-DIC. Therefore, we conclude that our instrument setup and technique have achieved the goal of better than ±0.05‰ for δ^{13}C-DIC precision recommended by Global Ocean Observing System[37] and have the possibility to be a convenient tool to measure the δ^{13}C-DIC samples both onboard and in the laboratory. However, as noted here, a suitable and long-term consistent standardization method is still to be evaluated. Currently, all our δ^{13}C-

293 DIC values are based on $NaHCO_3$ standards analyzed by the U.C. Davis Stable Isotope

294 Facility.

295 Table 2 The raw data of DIC and δ^{13}C-DIC in the multi-port valve test.

	δ^{13}C-DIC (‰)			DIC (μmol kg^{-1})		
Port	Round 1	Round 2	Round 3	Round 1	Round 2	Round 3
C	-3.93	-4.00	-3.98	2032.0	2033.0	2033.8
D	-3.97	-3.98	-3.97	2031.8	2033.3	2035.3
E	-3.94	-3.92	-3.98	2030.6	2034.4	2032.7
F	-3.91	-3.97	-3.97	2032.3	2032.7	2034.8
G	-3.94	-3.94	-3.97	2030.4	2031.6	2034.6
H	-3.88	-3.99	-4.02	2031.7	2031.7	2033.2
I	-3.95	-3.97	-3.98	2034.5	2032.7	2034.4
J	-3.91	-3.98	-3.96	2030.9	2034.7	2035.1
K	-4.00	-3.99	-3.95	2032.1	2034.6	2034.6
Average	*-3.94*	*-3.97*	*-3.98*	*2031.8*	*2033.2*	*2034.3*
STD	*0.04*	*0.02*	*0.02*	*1.2*	*1.2*	*0.9*
Average (all 3 rounds)		*-3.97*			*2033.1*	
STD (all 3 rounds)		*0.02*			*1.5*	

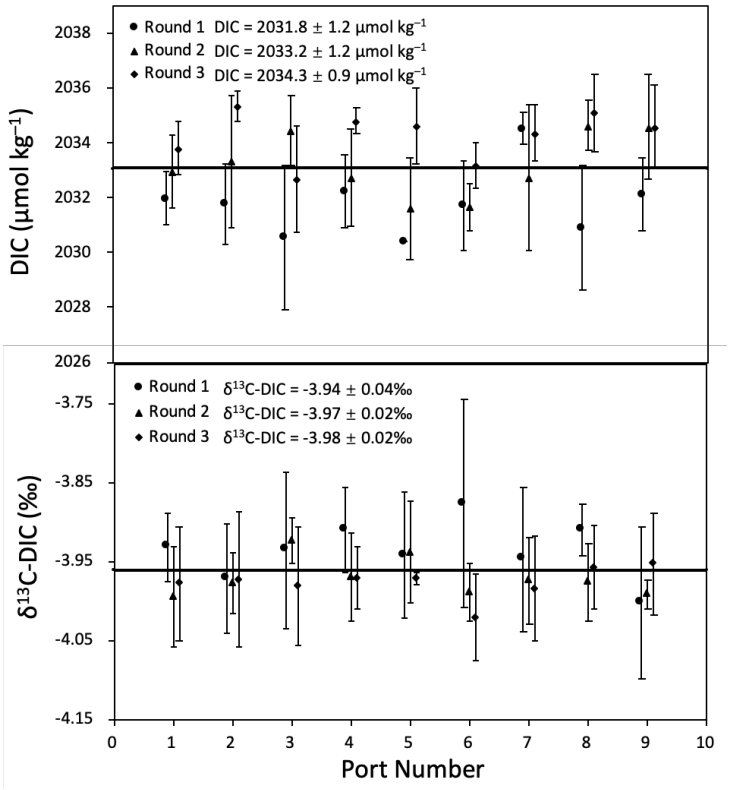

Fig. 3 Measured DIC concentrations (upper panel) and δ^{13}C-DIC values (lower panel) of the stock seawater using the upgraded multi-port valve. The solid lines in the two panels represent the averaged DIC concentration and δ^{13}C-DIC value from CRDS. Three rounds with three consecutive injections per port for nine ports were measured. The error bar is the standard deviations of the three consecutive injections at each port. This analytical procedure of three rounds lasted a total of about 20 hours.

This system is compact, both lab- and field-deployable, and analyzes DIC and δ^{13}C-DIC values without any sample pretreatment. In contrast, for offline IRMS δ^{13}C-DIC analysis, samples need to be acidified to liberate CO_2, which then goes through a vacuum line to be purified and concentrated into small vials before IRMS analysis[14]. However, our

method and system only need an operator to replace the samples once the previous batch analysis is completed. This automation avoids labor-intensive monitoring and operation, which allows for continuous measurements around the clock. Moreover, because instrument drift is low (DIC only drifted 0.059% and δ^{13}C-DIC drifted 0.047‰ within 3 weeks), the 3 standards are run only once a day or once every two days, after which all the time is dedicated to samples analysis in all nine sample channels. Note that, the standards and samples are run in a sequence each with three injections and a complete run average about 6 h. This results in a theoretical maximum throughput capacity of 37 samples with three injections (or 3 replicate measurements) each day (e.g., total 126 runs = (5 standards + 37 samples) × 3, and each run needs about 11 minutes).

However, our system normally analyzed less samples during routine sample analysis due to instrument down time over night and due to the intention of evaluating the system performance via analyzing multiple standards during the method development and evaluation stage. For example, during our recent analysis of 1200 samples from the California Current System (samples were taken during June—July and analysis was conducted during August—early November, 2021), 24 samples and two standards were analyzed each day with three shifts starting at ~8 am, ~3 pm and ~9 pm, respectively. During the overnight shift, the standards and some samples were analyzed twice. In addition to the home laboratory analysis, about 800 samples had been analyzed at sea onboard the research vessel Ron Brown during a 40-days cruise by two operators (on 12-

hour shifts). Compared with the analytical efficiency and application limitation of the IRMS instrument, our system greatly improves the spatial resolution of the $\delta^{13}C$-DIC samples.

One potential issue that could affect the sample repeatability is the sample temperature. Although the Picarro G2131-i detector has a built-in temperature control mode to ensure the detector operates under stable thermal conditions to minimize the temperature effect on CO_2 and isotope detection, environmental temperature variations will still influence the density of the water sample and result in the uncertainty of carbon content in a fixed injection sample volume. In our study, all measurements were conducted in a temperature-controlled room (T = 22 ± 1°C), where the 1°C temperature fluctuation will only cause a density change of 0.03% and an uncertainty of ± 0.5 μmol kg^{-1} in DIC concentration. It is smaller than the acceptable DIC precision of 2—4 μmol kg^{-1}, thus this temperature effect can be ignored. However, a water bath may be used onboard a ship or at a field laboratory to keep the sample temperature more stable.

3.2 Injection volume effect and concentration effect experiments

For the CRDS detector, the signals of CO_2 and $^{13}CO_2$ are determined by the carbon content liberated from water sample, rather than solely by the DIC concentration or injection volume. A smaller injection volume with a fixed DIC concentration or a lower DIC concentration with a fixed injection volume would result in a smaller integrated net area and a lower CO_2 peak and less distributed points of $^{13}CO_2$ above the cutoff value,

thereby potentially reducing the precision of δ^{13}C-DIC. For example, with a fixed DIC concentration, the uncertainty of δ^{13}C-DIC will increase as the injection volume decreases, which is known as injection volume effect. With a fixed injection volume, δ^{13}C-DIC uncertainty is less than ± 0.2‰ when DIC concentration is above 360 μmol kg^{-1}, whereas it rapidly increases to >0.5‰ when DIC concentration is <130 μmol kg^{-1} in the study by Bass et al.[21], which is known as the concentration effect. The same is true in our analysis. As an extreme case in our analysis, if the entire CO_2 curve is less than the cutoff CO_2 value, there will be no valid δ^{13}C-DIC. If there is only a small fraction of the CO_2 curve near the peak above the cutoff line, then, one would expect a higher uncertainty in the derived δ^{13}C-DIC.

To examine the potential volume effect on the performance of the analyzer, we analyzed the same seawater with 24 different sample volumes (again each volume had three consecutive injections). The pooled averaged DIC concentration was 2355.8 ± 2.8 μmol kg^{-1} as determined by reference to CRM #185 (Fig. 4b), which is close to the value (2353.1 ± 0.4 μmol kg^{-1}) measured by the traditional NDIR method[30]. Except for a few points near the low injection volume, all the DIC data fall within the precision range of ± 0.2%, which is only slightly higher than that of the traditional NDIR method[30]. The averaged δ^{13}C-DIC was -5.56 ± 0.06‰ (Fig. 4a), again with high precision same as that in the multi-port evaluation. To be specific, 77.8% of the δ^{13}C-DIC data located in the averaged ±1σ ranges if following our system precision (0.06%) while 91.7% of δ^{13}C-DIC data fall in the

averaged ±1σ ranges according to the precision (0.09%) of Su et al.[6]. We suggests that our measurement system is still stable even if the injection volume varies greatly. As mentioned above, the CO_2 and $^{13}CO_2$ signal are measured based on the carbon content of a sample. In the injection volume and concentration effect experiments, DIC and its δ^{13}C-DIC data are basically stable in a wide range of injection volume, which could be attributed to the fact that the stock seawater used in this experiment represents the typical open ocean water and has a high carbon content (DIC = 2355.8 μmol kg^{-1}). However, if estuarine water (such as DIC = ~1000 μmol kg^{-1} or less) is used for this experiment, the stability of δ^{13}C-DIC will be poor due to its low carbon content and few data points above the cutoff line. Therefore, the injection volume has a significant influence on the estuarine and riverine water with low DIC concentrations and a large injection volume will be needed to analyze δ^{13}C-DIC with high precision and accuracy.

For the concentration effect experiment, the δ^{13}C-DIC value exhibited a decreasing trend with a decreased DIC concentration, and the δ^{13}C-DIC became slightly depleted when DIC concentration decreased to 247 μmol kg^{-1} (Fig. 4c). The standard deviation of all δ^{13}C-DIC values was 0.20‰, which is not negligible given that the measurement precision of our measurement system is better than 0.06‰. However, besides the lowest concentration of 247 μmol kg^{-1}, the isotope precision variation was small and better than 0.10‰ when DIC concentration ranged from 536 to 2283 μmol kg^{-1} (Fig. 4d), which is similar to the precision of Su et al.[6] and also closer to our system precision. The lower δ^{13}C-

DIC in lower DIC concentration could likely be attributed to the invasion of atmospheric CO_2 with lighter isotope during the pre-treatment process of the stock seawater dilution, which thus has a significant concentration effect on lower DIC concentration samples, compared with higher DIC concentration samples as Call et al.[22] suggested before. Similarly, an obviously negative correlation between δ^{13}C-DIC values and DIC concentrations in the concentration effect for δ^{13}C-DIC experiment in Cheng et al.[26] also verified the invasion of atmospheric CO_2 in the preparation of a set of $NaHCO_3$ standard solution, since atmospheric CO_2 has a heavier isotope compared with -21.04‰ $NaHCO_3$[26].

Here we offer an alternative explanation. As the carbon amount becomes lower either because of low sample volume or low DIC concentration, the weight of $\delta^{13}CO_2$ with higher instrument noise at lower $^{12}CO_2$ concentration (near 350 ppm) becomes more significant. We have noticed that such noise at low CO_2 level of a Picarro instrument is not necessarily random and may be instrument specific (for the two G2131-i units in our laboratory, one goes to more positive and another goes to more negative). Thus, we recommend maximizing the sample volume when DIC concentration of the sample is low.

While not fully and purposely evaluated, results from the volume and concentration experiments also indicate that there is no visible isotope fractionation effect in our instrument and method. Since we have selected a fixed criteria for ending sample analysis (when baseline after the peak is < 5 ppm CO_2 above the baseline before the peak) and the cutoff CO_2 reading for averaging the $\delta^{13}CO_2$ value is fixed at 350 ppm (though both are

user definable), the higher the DIC amount in the sample (either larger volume or higher concentration or both), the less $\delta^{13}CO_2$ signal is lost in counting towards the final δ^{13}C-DIC value. The fact that no statistically significant difference is observed beyond ±0.06‰ when seawater sample volume is > 2 mL (when DIC about 2000 µmol kg^{-1}) suggests that no significant isotope fractionation occurs in our method. It also appears that the same conclusion can be drawn for estuarine and freshwater analysis when the DIC concentration is above 500 µmol kg^{-1} (injection volume is 3.5 mL) and a slightly larger uncertainly of ± 0.1‰ uncertainty is permitted. For analysis of freshwater samples with lower DIC, we recommend using a larger sample injection volume of 5.0 mL or greater.

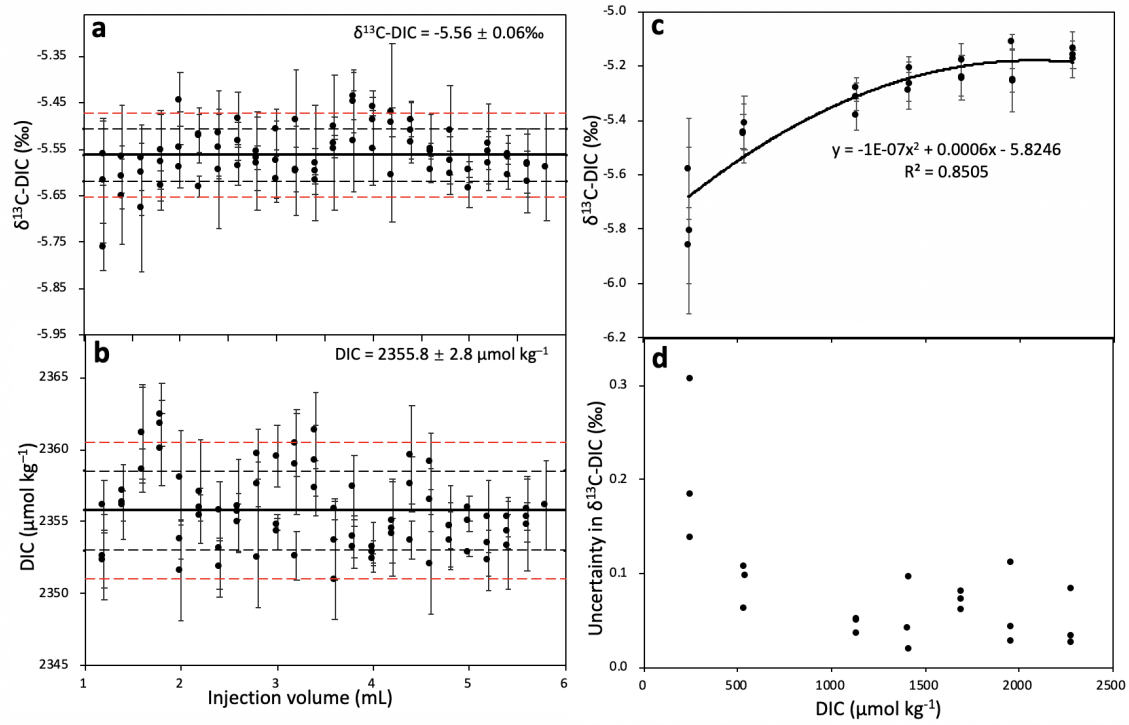

Fig. 4 δ^{13}C-DIC values and its precision (a) as well as measured DIC concentrations (b) of the aged seawater in the injection volume effect experiment; concentration effect on δ^{13}C-

DIC values (c) and δ^{13}C-DIC uncertainty vs. DIC concentration (d) in the concentration effect experiment. In Fig (a) and (b), the black solid-lines indicate the averaged values of δ^{13}C-DIC values and DIC concentrations; For all data, the black dashed-lines represent 1 σ standard deviation interval; the red dashed-lines indicate 0.09‰ range for δ^{13}C-DIC and 2 σ standard deviation interval for DIC. In Fig (c), the black curve represents the relationship between the δ^{13}C-DIC values and DIC concentrations. Note that these two experiments were two separate sets that ran on different days and were merged here together. Each injection volume and concentration have three repeat samples, and error bar means the standard deviations of the three injections for each sample. Specifically, the injection volume effect experiment lasted about 64 hours and the concentration effect experiment lasted about 35 hours, the instrument always ran well during the intervals of these days (7 days).

3.3 Carbonate system in the Delaware Estuary

Compared with other systems like the Chesapeake Bay, the physical circulation and hydrology in the Delaware Estuary are relatively simple, because the major inflow is a single river and water is generally vertically well-mixed[38]. Thus, the Delaware Estuary is an ideal site for method development and evaluation, and has served this purpose well as a backyard laboratory for researchers at the University of Delaware for decades[28,29,38–41].

The measured DIC and TA, pH_25°C and δ^{13}C-DIC increased while underway pCO_2 decreased with the increasing salinity from the upper tidal river to the low bay (Fig. 5). Specifically, from the river end to the ocean end, DIC increased from 970.6 to 1975.0 μmol kg^{-1}, TA increased from 944.6 to 2150.5 μmol kg^{-1}, and δ^{13}C-DIC increased from -9.57 to 0.37‰. DIC and TA had slightly higher values than the conservative mixing lines in the turbidity maximum zone. However, DIC concentrations were slightly lower than the conservative mixing line and TA values followed the conservative mixing line in the mid-salinity upper bay (Fig. 5a).

The δ^{13}C-DIC values along the salinity gradient were depleted in the freshwater areas, while enriched in the mid-salinity zone of the estuary (Fig. 5b). The pH_25°C and underway pCO_2 values were in the ranged from 7.61–8.10 and 1010–258 μatm, respectively, with marked salinity gradient changing from 0.16 to 30.54 (Figs. 5b and 5a). To be specific, pH increased from 7.61 in the Delaware River up to 8.10 in the upper bay, then decreased slightly to 7.95 in the marine part of the estuary. Compared to the atmospheric level (422 μatm), pCO_2 was obviously supersaturated (>500 μatm) in the turbidity maximum zone and then decreased to undersaturated in the mid and low bay. Consistent with pH distribution, pCO_2 value was lowest in the mid-salinity upper bay and slightly increased to near the atmospheric CO_2 level in the lower bay (Fig. 5a). Overall, the Delaware Estuary is characterized as a strong CO_2 source to the atmosphere in the river

456 end and at the turbidity maximum zone and a weak CO_2 sink in the mid and lower bays
457 during springtime. This observation is consistent with the investigation of Joesoef et al.[40].

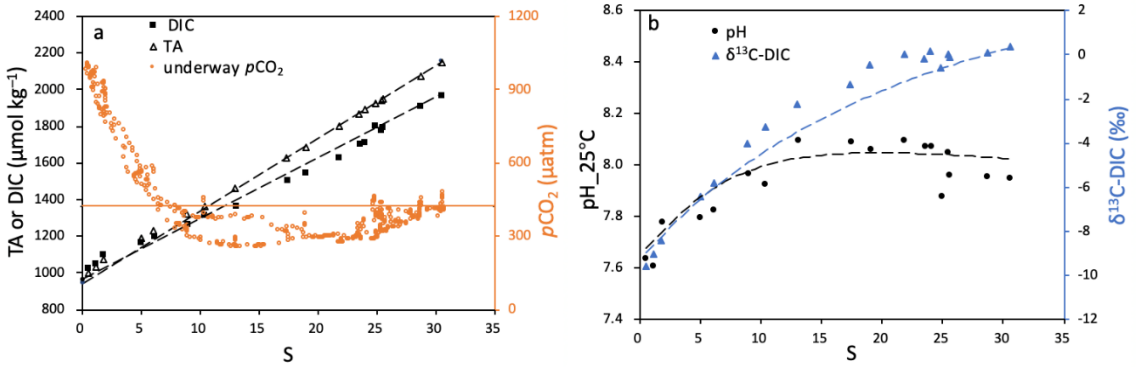

458

459 **Fig. 5** Distributions of DIC and TA concentrations and underway pCO_2 (a), pH_25°C and
460 δ^{13}C-DIC (b) against salinity. In Fig. 5a, the black dashed lines are the DIC and TA
461 conservative mixing lines, the orange horizontal line represents the atmospheric pCO_2 level;
462 In Fig. 5b, the black and blue dashed curves are the pH and δ^{13}C-DIC conservative mixing
463 lines, respectively. The DIC, TA, pH_25°C and δ^{13}C-DIC conservative mixing lines are
464 specified in section 2.5.

465 While it is clear that physical mixing plays the most important role in the Delaware
466 Estuary, the deviations of carbonate parameters from the conservative mixing lines (Fig. 5)
467 indicate that processes other than physical mixing also play an important role in regulating
468 their distributions in the estuary. While DIC distribution and dynamics have been studied
469 by Joesoef et al.[39], δ^{13}C-DIC has not been studied and could add an important constraint to
470 identifying biogeochemical mechanisms important in controlling the carbon cycling and
471 air-sea CO_2 flux. Therefore, in order to discuss the influencing mechanism of other

processes on the DIC and its isotope distributions in the Delaware Estuary, the deviations of DIC concentrations and δ^{13}C-DIC signals from the above conservative mixing lines are used here for discussion, since the processes affecting DIC will have distinct δ^{13}C-DIC source values and isotope fractionation. Following the method described in Alling et al.[1], the deviations of DIC concentrations and δ^{13}C-DIC signals from their conservative mixing lines (Equations 4 and 5) can be calculated by the equations:

$$\Delta DIC = \frac{DIC_{meas} - DIC_{mix}}{DIC_{mix}} \quad (6)$$

$$\Delta\delta^{13}C\text{-}DIC = \delta^{13}C\text{-}DIC_{meas} - \delta^{13}C\text{-}DIC_{mix} \quad (7)$$

Where DIC_{mix} and $\delta^{13}C\text{-}DIC_{mix}$ are given in Equation 4 and 5, respectively. The main biogeochemical mechanisms affecting the distributions of δ^{13}C-DIC and DIC could be inferred by the slopes of the relationship between $\Delta\delta^{13}$C-DIC and ΔDIC (Fig. 6).

Stations near the Delaware River fall within quadrant IV, which is characterized by the strong DIC addition and δ^{13}C-DIC depletion. It represents the influence of terrestrial organic matter degradation and is confirmed by the oversaturated pCO_2 relative to atmospheric CO_2 (Fig. 5a) and relatively low pH (Fig. 5b)[42–44]. Meanwhile, low aragonite saturation state ($\Omega_{arag.}$ <0.37, Fig. 7) near the freshwater area indicates that $CaCO_3$ dissolution might also occur, which added to both DIC and TA, and in the meantime, enriched the δ^{13}C-DIC value by releasing the ^{13}C-enriched carbonate and bicarbonate ions into the water column DIC pool[3]. Therefore, the points in quadrant IV slightly deviate from the theoretical vector of terrestrial organic matter decomposition from the river source and

492 shifted upward to the direction of the vector of $CaCO_3$ dissolution. Note that while the
493 stoichiometric ratio of ΔTA to ΔDIC should be 2:1 during $CaCO_3$ dissolution, if the
494 dissolution is driven by metabolically produced CO_2 input, then the ratio would be nearly
495 or less than 1:1 (i.e., metabolic carbonate dissolution, $CaCO_3 + CH_2O + O_2 + H_2O \rightarrow Ca^{2+}$
496 $+ 2HCO_3^-$)[45], which occurs in the freshwater member with S<3 (Fig. 7).

497 The turbidity maximum zone stations are in the lower portion of quadrant I, mainly
498 affected by $CaCO_3$ dissolution of suspended particulate matter and organic matter
499 degradation. Additional evidence supporting the $CaCO_3$ dissolution mechanism is the
500 substantial additions of DIC and TA in the low salinity region (Fig. 7). The excess TA
501 ($\Delta TA = TA_{meas} - TA_{mixing}$) in and near the turbidity maximum zone (5< S <10) may mainly
502 come from the $CaCO_3$ dissolution. Here the ΔTA to ΔDIC ratio ranges 1.3-1.7 and is much
503 higher than those at or near the river endmember (S<2) (Fig. 7). Therefore, the variations
504 of DIC and δ^{13}C-DIC in the turbidity maximum zone were mainly controlled by the
505 combined effects of organic carbon degradation from rivers and $CaCO_3$ dissolution.

506 Almost all stations in the Delaware Bay, including the upper bay and the lower bay,
507 are in quadrant II. The Delaware Estuary has an inverted funnel shape, and the upper bay
508 is below the neck of funnel, where the bay becomes wider, water flow slows down, clarity
509 improves and biological production increases[28,39,40]. In addition, small scale spring blooms
510 with high primary production usually occur in the Delaware Bay in March and April,
511 especially in the upper bay[46]. The high primary production, associated with DIC uptake,

512 preferentially removes lighter ^{12}C and enriches the water with the heavier stable carbon
513 isotope[47]. Considering high biomass and primary productivity lead to undersaturated or
514 nearly equilibrated pCO_2 relative to the atmospheric CO_2, there should be no impact from
515 CO_2 outgassing. In addition, Stations 15 and 9 in the upper portion of the upper bay fall in
516 the upper portion of quadrant I, which is dominated by the combined factors of primary
517 production and $CaCO_3$ dissolution ($\Omega_{arag.}$= 0.6 and 1.0, Fig. 7). Therefore, DIC loss and
518 elevated $\delta^{13}C$-DIC in the upper Delaware Bay are mainly attributed to primary production
519 and $CaCO_3$ dissolution.

520 Although our calculations are associated with some uncertainties and limitations, the
521 approach used in this study certainly provides a new insight into the sources and cycling
522 of DIC in the Delaware Estuary and serves as a good example of using DIC concentrations
523 and $\delta^{13}C$-DIC values to study biogeochemical processes in aquatic systems. The deviations
524 of DIC and $\delta^{13}C$-DIC from conservative mixing lines can be regarded as fingerprints left
525 by different biogeochemical processes. Overall, the variations of the carbonate system are
526 primarily controlled by the physical mixing in the Delaware Estuary. Besides that, the
527 control mechanisms in the Delaware River and turbidity maximum zone are the combined
528 effects of the degradation of organic carbon and carbonate dissolution, but are dominated
529 by primary production in the Delaware Bay. The relative importance of these processes
530 changes over seasons, which will be the subject of a subsequent publication.

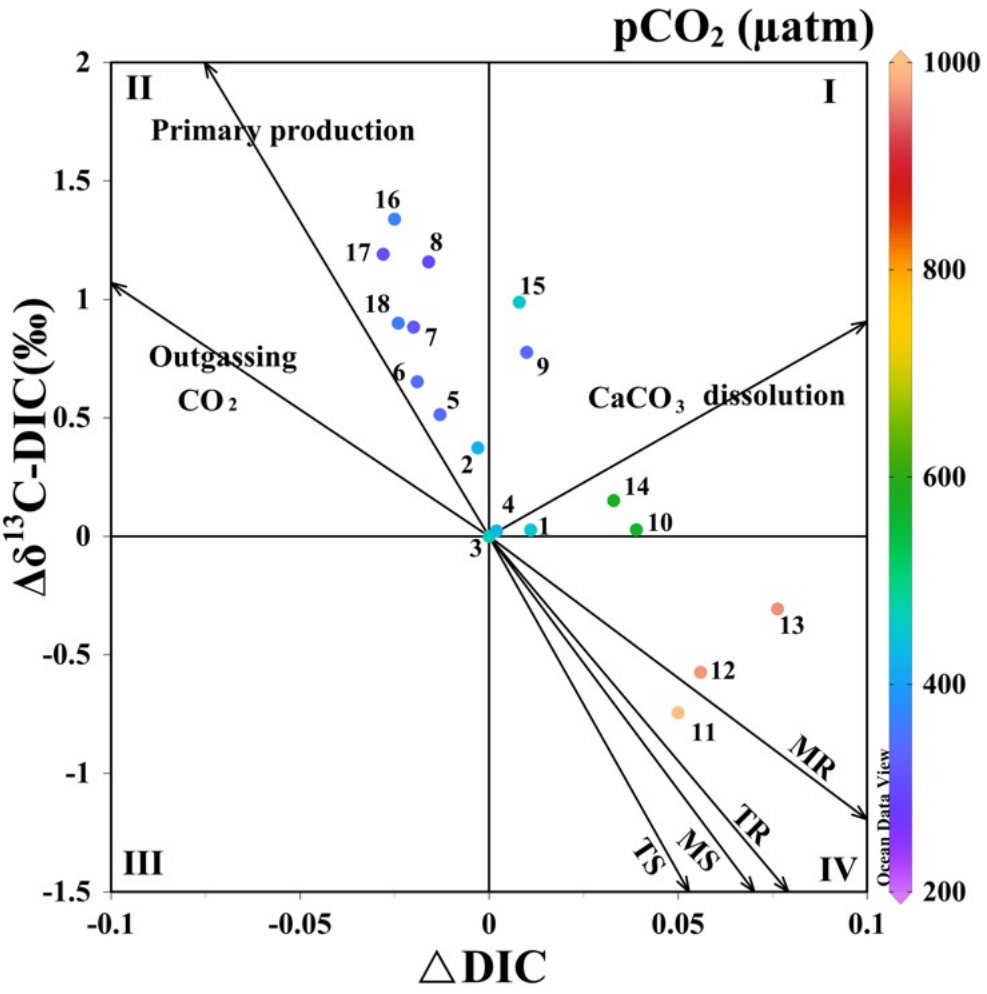

Fig. 6 The absolute changes of δ^{13}C-DIC ($\Delta\delta^{13}$C-DIC) and the relative changes of DIC concentration (ΔDIC) relative to the conservative mixing lines in the Delaware Estuary in April 2019. The origin represents the data only controlled by physical mixing. The figure is divided into four quadrants, each indicating the position of samples whose DIC concentration and δ^{13}C-DIC were influenced by additional processes (non-physical mixing process). Quadrant I represents carbonate dissolution when both DIC and δ^{13}C-DIC increase; quadrant II represents primary production or CO_2 outgassing when DIC decreases while δ^{13}C-DIC increases; quadrant III represents calcite precipitation when both DIC and

δ^{13}C-DIC decrease; quadrant IV represents degradation of organic carbon when DIC increases but δ^{13}C-DIC decreases. The vectors indicate the effects of most likely processes affecting DIC. Four vectors in quadrant IV indicate four possible effects of organic matter degradation, which depend on the sources of organic carbon (T: terrestrial source; M: marine source) and the initial DIC and δ^{13}C-DIC composition in the water (S: seawater; R: river water). MR (or TR) stands for CO_2 addition from the decomposition of marine (or terrestrial) organic matter to river water and MS (or TS) stands for CO_2 addition from the decomposition of marine (or terrestrial) organic matter to seawater. Arabic numerals in the figure represent the sampling stations. The calculations of all vectors are based on Samanta et al.[3].

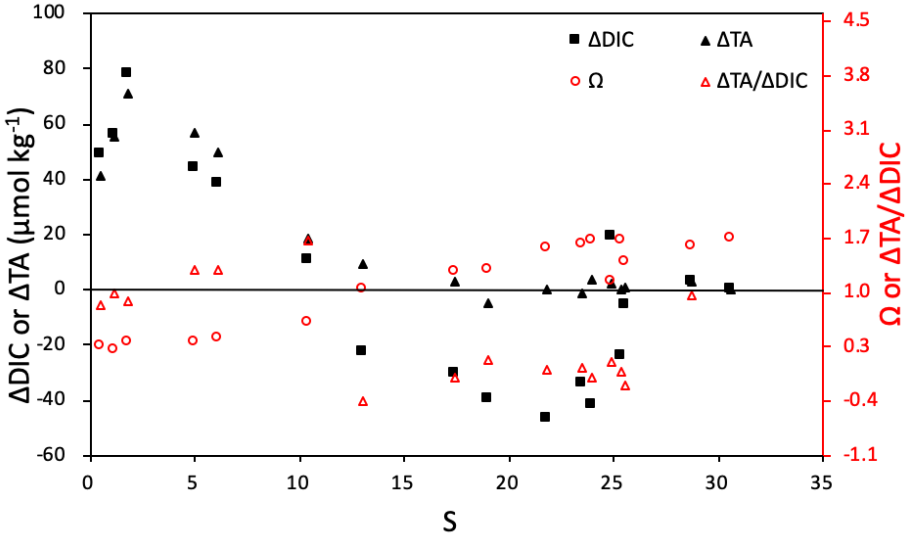

Fig. 7 The TA and DIC differences between measured and conservative mixing values (ΔTA and ΔDIC, left axis), aragonite saturation (Ω, right axis) and the ratio of ΔTA and ΔDIC (ΔTA/ΔDIC, right axis) against salinity. The black dashed horizontal line represents

554 both the 0-reference line of ΔTA or ΔDIC, and the 1.0 aragonite saturation line. Data (solid
555 square and triangle symbol) above the line mean addition, while beneath the line indicate
556 removal of DIC or TA. Also, data (open circle symbol) above the line indicate calcium
557 carbonate precipitation but dissolution below the line.

558 **4 Conclusion**

559 Here we extensively evaluated the performance of a method where we coupled a CO_2
560 extraction device with a multi-port sample valve and a CRDS detector to simultaneously
561 analyze DIC concentrations and δ^{13}C-DIC values with high precision (better than ± 1.95
562 μmol kg^{-1} for DIC concentration and better than ± 0.06‰ for δ^{13}C-DIC). The highlight of
563 this instrument configuration is an upgraded multi-sample valve compared to a single-
564 sample valve used in Su et al.[6]. The instrument setup can potentially analyze about 37
565 samples per day with three replicate measurements and achieve continuous measurements
566 around the clock, which is convenient and labor-saving during analysis. Moreover, the
567 instrument can be used in a land-based laboratory, at sea or at a field station. For the coastal
568 and open ocean waters with high DIC concentration, the choice of injection volume has
569 little impact on the δ^{13}C-DIC sample determination. However, we recommend using a large
570 injection volume for samples with low DIC concentration to minimize the influence of low
571 injection volume on the δ^{13}C-DIC precision.

572 This technique was applied in the Delaware Estuary in Spring of 2019 to determine
573 the spatial distributions of DIC concentration and δ^{13}C-DIC and to understand the
574 controlling mechanisms. The relationship between ΔDIC and $\Delta\delta^{13}$C-DIC demonstrated
575 that, in addition to estuarine mixing, they were primarily controlled by the degradation of
576 organic carbon and carbonate dissolution in the Delaware River and turbidity maximum
577 zone, but mainly by primary production in the Delaware Bay. This application provides a
578 new insight for distinguishing the control mechanisms on DIC and δ^{13}C-DIC in the
579 Delaware Estuary. The application of this measuring system could rapidly expand the
580 temporal and spatial coverages of the paired DIC concentration and δ^{13}C-DIC in the
581 fieldwork, thereby facilitating further the understanding of the underlying biogeochemical
582 processes and controls on air-sea CO_2 flux and acidification in different aquatic
583 environments.

Acknowledgements

We thank UC Davis Stable Isotope Facility for verifying the δ^{13}C-DIC values of samples using the isotope-ratio mass spectrometry, and the engineers at Apollo SciTech for the upgrade of the system hardware and software. Special thanks to Dr. Najid Hussain for the logistics assistance during the laboratory experiments and Dr. Amanda Timmerman for English editing. We are also grateful to Xinyu Li for discussion. This work was supported by a Delaware Bioscience Center for Advanced Technology (CAT) Applied Research Collaborations (ARC) award, NSF Delaware EPSCoR project, and NSF OCE-2123768. X. Deng thanks the China Scholarship Council for providing the scholarship fund (No. 20180633027). W. -J. Cai is related to the Apollo SciTech.

References:

(1) Alling, V.; Porcelli, D.; Mörth, C. M.; Anderson, L. G.; Sanchez-Garcia, L.; Gustafsson, Ö.; Andersson, P. S.; Humborg, C. Degradation of Terrestrial Organic Carbon, Primary Production and Out-gassing of CO_2 in the Laptev and East Siberian Seas as Inferred from $\delta^{13}C$ Values of DIC. *Geochim. Cosmochim. Acta* **2012**, *95*, 143–159. https://doi.org/10.1016/j.gca.2012.07.028.

(2) Hellings, L.; Dehairs, F.; Tackx, M.; Keppens, E.; Baeyens, W. Origin and Fate of Organic Carbon in the Freshwater Part of the Scheldt Estuary as Traced by Stable Carbon Isotope Composition. *Biogeochemistry* **1999**, *47* (2), 167–186. https://doi.org/10.1007/BF00994921.

(3) Samanta, S.; Dalai, T. K.; Pattanaik, J. K.; Rai, S. K.; Mazumdar, A. Dissolved Inorganic Carbon (DIC) and Its $\delta^{13}C$ in the Ganga (Hooghly) River Estuary, India: Evidence of DIC Generation via Organic Carbon Degradation and Carbonate Dissolution. *Geochim. Cosmochim. Acta* **2015**, *165*, 226–248. https://doi.org/10.1016/j.gca.2015.05.040.

(4) Schulte, P.; van Geldern, R.; Freitag, H.; Karim, A.; Négrel, P.; Petelet-Giraud, E.; Probst, A.; Probst, J.-L.; Telmer, K.; Veizer, J.; Barth, J. A. C. Applications of Stable Water and Carbon Isotopes in Watershed Research: Weathering, Carbon Cycling, and Water Balances. *Earth-Sci. Rev.* **2011**, *109* (1–2), 20–31. https://doi.org/10.1016/j.earscirev.2011.07.003.

(5) Su, J.; Dai, M.; He, B.; Wang, L.; Gan, J.; Guo, X.; Zhao, H.; Yu, F. Tracing the Origin of the Oxygen-consuming Organic Matter in the Hypoxic Zone in a Large Eutrophic Estuary: The Lower Reach of the Pearl River Estuary, China. *Biogeosciences* **2017**, *14* (18), 4085–4099. https://doi.org/10.5194/bg-14-4085-2017.

(6) Su, J.; Cai, W.-J.; Hussain, N.; Brodeur, J.; Chen, B.; Huang, K. Simultaneous Determination of Dissolved Inorganic Carbon (DIC) Concentration and Stable Isotope (δ^{13}C-DIC) by Cavity Ring-Down Spectroscopy: Application to Study Carbonate Dynamics in the Chesapeake Bay. *Mar. Chem.* **2019**, *215*, 103689. https://doi.org/10.1016/j.marchem.2019.103689.

(7) Wang, H.; Dai, M.; Liu, J.; Kao, S.-J.; Zhang, C.; Cai, W.-J.; Wang, G.; Qian, W.; Zhao, M.; Sun, Z. Eutrophication-Driven Hypoxia in the East China Sea off the Changjiang Estuary. *Environ. Sci. Technol.* **2016**, *50* (5), 2255–2263. https://doi.org/10.1021/acs.est.5b06211.

(8) Xuan, Y.; Cao, Y.; Tang, C.; Li, M. Changes in Dissolved Inorganic Carbon in River Water Due to Urbanization Revealed by Hydrochemistry and Carbon Isotope in the Pearl River Delta, China. *Environ. Sci. Pollut. Res.* **2020**, *27*, 24542–24557. https://doi.org/10.1007/s11356-020-08454-4.

(9) Quay, P. D.; Stutsman, J.; Feely, R. A.; Juranek, L. W. Net Community Production Rates across the Subtropical and Equatorial Pacific Ocean Estimated from Air-Sea

δ^{13}C Disequilibrium. *Global Biogeochem. Cycles* **2009**, *23* (2), GB2006. https://doi.org/10.1029/2008GB003193.

(10) Gruber, N.; Keeling, C. D.; Stocker, T. F. Carbon-13 Constraints on the Seasonal Inorganic Carbon Budget at the BATS Site in the Northwestern Sargasso Sea. *Deep Sea Res. I* **1998**, *45* (4), 673–717. https://doi.org/10.1016/S0967-0637(97)00098-8.

(11) Quay, P.; Sonnerup, R.; Westby, T.; Stutsman, J.; McNichol, A. Changes in the $^{13}C/^{12}C$ of Dissolved Inorganic Carbon in the Ocean as a Tracer of Anthropogenic CO_2 Uptake. *Global Biogeochem. Cycles* **2003**, *17* (1), 1004. https://doi.org/10.1029/2001GB001817.

(12) Quay, P.; Sonnerup, R.; Munro, D.; Sweeney, C. Anthropogenic CO_2 Accumulation and Uptake Rates in the Pacific Ocean Based on Changes in the $^{13}C/^{12}C$ of Dissolved Inorganic Carbon. *Global Biogeochem. Cycles* **2017**, *31* (1), 59–80. https://doi.org/10.1002/2016GB005460.

(13) Atekwana, E. A.; Krishnamurthy, R. V. Extraction of Dissolved Inorganic Carbon (DIC) in Natural Waters for Isotopic Analyses. In *Handbook of Stable Isotope Analytical Techniques*; **2004**; pp 203–228.

(14) Humphreys, M. P.; Achterberg, E. P.; Griffiths, A. M.; McDonald, A.; Boyce, A. J. Measurements of the Stable Carbon Isotope Composition of Dissolved Inorganic Carbon in the Northeastern Atlantic and Nordic Seas during Summer 2012. *Earth Syst. Sci. Data* **2015**, *7*, 127–135. https://doi.org/10.5194/essd-7-127-2015.

(15) Salata, G. G.; Roelke, L. A.; Cifuentes, L. A. A Rapid and Precise Method for Measuring Stable Carbon Isotope Ratios of Dissolved Inorganic Carbon. *Mar. Chem.* **2000**, *69* (1), 153–161. https://doi.org/10.1016/S0304-4203(99)00102-4.

(16) Torres, M. E.; Mix, A. C.; Rugh, W. D. Precise $\delta^{13}C$ Analysis of Dissolved Inorganic Carbon in Natural Waters Using Automated Headspace Sampling and Continuous-Flow Mass Spectrometry. *Limnol. Oceanogr. Methods* **2005**, *3* (8), 349–360. https://doi.org/10.4319/lom.2005.3.349.

(17) Waldron, S.; Scott, E. M.; Vihermaa, L. E.; Newton, J. Quantifying Precision and Accuracy of Measurements of Dissolved Inorganic Carbon Stable Isotopic Composition Using Continuous-Flow Isotope-Ratio Mass Spectrometry. *Rapid Commun. Mass Spectrom.* **2014**, *28* (10), 1117–1126. https://doi.org/10.1002/rcm.6873.

(18) Friedrichs, G.; Bock, J.; Temps, F.; Fietzek, P.; Körtzinger, A.; Wallace, D. W. R. Toward Continuous Monitoring of Seawater $^{13}CO_2/^{12}CO_2$ Isotope Ratio and pCO_2: Performance of Cavity Ringdown Spectroscopy and Gas Matrix Effects. *Limnol. Oceanogr. Methods* **2010**, *8* (10), 539–551. https://doi.org/10.4319/lom.2010.8.539.

(19) Becker, M.; Andersen, N.; Fiedler, B.; Fietzek, P.; Körtzinger, A.; Steinhoff, T.; Friedrichs, G. Using Cavity Ringdown Spectroscopy for Continuous Monitoring of $\delta^{13}C$ (CO_2) and fCO_2 in the Surface Ocean. *Limnol. Oceanogr.: Methods* **2012**, *10*, 752–766. https://doi.org/10.4319/lom.2012.10.752.

(20) Becker, M.; Andersen, N.; Erlenkeuser, H.; Humphreys, M. P.; Tanhua, T.; Körtzinger, A. An Internally Consistent Dataset of δ^{13}C-DIC in the North Atlantic Ocean–NAC13v1. *Earth Syst. Sci. Data* **2016**, *8* (2), 559–570. https://doi.org/10.5194/essd-8-559-2016.

(21) Bass, A. M.; Bird, M. I.; Munksgaard, N. C.; Wurster, C. M. ISO-CADICA: Isotopic–Continuous, Automated Dissolved Inorganic Carbon Analyser. *Rapid Commun. Mass Spectrom.* **2012**, *26* (6), 639–644. https://doi.org/10.1002/rcm.6143.

(22) Call, M.; Schulz, K. G.; Carvalho, M. C.; Santos, I. R.; Maher, D. T. Technical Note: Coupling Infrared Gas Analysis and Cavity Ring down Spectroscopy for Autonomous, High-Temporal-Resolution Measurements of DIC and δ^{13}C–DIC. *Biogeosciences* **2017**, *14* (5), 1305–1313. https://doi.org/10.5194/bg-14-1305-2017.

(23) Dickinson, D.; Bodé, S.; Boeckx, P. System for δ^{13}C–CO_2 and $x$$CO_2$ Analysis of Discrete Gas Samples by Cavity Ring-down Spectroscopy. *Atmos. Meas. Tech.* **2017**, *10* (11), 4507–4519. https://doi.org/10.5194/amt-10-4507-2017.

(24) Dickinson, D.; Bodé, S.; Boeckx, P. Measuring ^{13}C-Enriched CO_2 in Air with a Cavity Ring-down Spectroscopy Gas Analyser: Evaluation and Calibration. *Rapid Commun. Mass Spectrom.* **2017**, *31* (22), 1892–1902. https://doi.org/10.1002/rcm.7969.

(25) López-Sandoval, D. C.; Delgado-Huertas, A.; Carrillo-de-Albornoz, P.; Duarte, C. M.; Agustí, S. Use of Cavity Ring-down Spectrometry to Quantify ^{13}C-Primary

693 Productivity in Oligotrophic Waters. *Limnol. Oceanogr. Methods* **2019**, *17* (2), 137–
694 144. https://doi.org/10.1002/lom3.10305.
695 (26) Cheng, L.; Normandeau, C.; Cai, W.-J.; Wallace, D. Shipboard Measurement of DIC
696 and δ^{13}C-DIC on Discrete Seawater Samples Using Cavity Ring-Down Spectroscopy:
697 System Testing and Performance during Three Research Cruises in the North Atlantic.
698 *Isot. Environ. Health Stud.* **2021**. (Accept)
699 (27) Dickson, A. G.; Sabine, C. L.; Christian, J. R. *Guide to Best Practices for Ocean CO_2*
700 *Measurements*; PICES Special Publication 3, 191pp, **2007**.
701 (28) Sharp, J. H. Estuarine Oxygen Dynamics: What Can We Learn about Hypoxia from
702 Long-Time Records in the Delaware Estuary? *Limnol. Oceanogr.* **2010**, *55* (2), 535–
703 548. https://doi.org/10.4319/lo.2010.55.2.0535.
704 (29) Sharp, J. H.; Yoshiyama, K.; Parker, A. E.; Schwartz, M. C.; Curless, S. E.;
705 Beauregard, A. Y.; Ossolinski, J. E.; Davis, A. R. A Biogeochemical View of
706 Estuarine Eutrophication: Seasonal and Spatial Trends and Correlations in the
707 Delaware Estuary. *Estuaries Coasts* **2009**, *32* (6), 1023–1043.
708 https://doi.org/10.1007/s12237-009-9210-8.
709 (30) Huang, W.-J.; Wang, Y.; Cai, W.-J. Assessment of Sample Storage Techniques for
710 Total Alkalinity and Dissolved Inorganic Carbon in Seawater: Sample Storage
711 Techniques for TA and DIC. *Limnol. Oceanogr. Methods* **2012**, *10* (9), 711–717.
712 https://doi.org/10.4319/lom.2012.10.711.

(31) Chen, B.; Cai, W.-J.; Brodeur, J. R.; Hussain, N.; Testa, J. M.; Ni, W.; Li, Q. Seasonal and Spatial Variability in Surface pCO_2 and Air–Water CO_2 Flux in the Chesapeake Bay. *Limnol. Oceanogr.* **2020**, *65* (12), 3046–3065. https://doi.org/10.1002/lno.11573.

(32) Kanamori, S.; Ikegami, H. Computer-Processed Potentiometric Titration for the Determination of Calcium and Magnesium in Sea Water. *J. Oceanogr. Soc.Jpn* **1980**, *36*, 177–184. https://doi.org/10.1007/bf02070330.

(33) Mucci, A. The Solubility of Calcite and Aragonite in Seawater at Various Salinities, Temperatures, and One Atmosphere Total Pressure. *Am. J. Sci.* **1983**, *283* (7), 780–799. https://doi.org/10.2475/ajs.283.7.780.

(34) Su, J.; Cai, W.-J.; Brodeur, J.; Hussain, N.; Chen, B.; Testa, J. M.; Scaboo, K. M.; Jaisi, D. P.; Li, Q.; Dai, M.; Cornwell, J. Source Partitioning of Oxygen-Consuming Organic Matter in the Hypoxic Zone of the Chesapeake Bay. *Limnol. Oceanogr.* **2020**, *65* (8), 1801–1817. https://doi.org/10.1002/lno.11419.

(35) Fry, B. Conservative Mixing of Stable Isotopes across Estuarine Salinity Gradients: A Conceptual Framework for Monitoring Watershed Influences on Downstream Fisheries Production. *Estuaries* **2002**, *25* (2), 264–271. https://doi.org/10.1007/BF02691313.

(36) Pierrot, D.; Lewis, E.; Wallace, D. W. R. MS Excel Program Developed for CO_2 System Calculations. *ORNL/CDIAC-105a. Carbon Dioxide Information Analysis*

Center, Oak Ridge National Laboratory, US Department of Energy, Oak Ridge, Tennessee **2006**.

(37) Cheng, L.; Normandeau, C.; Bowden, R.; Doucett, R.; Gallagher, B.; Gillikin, D. P.; Kumamoto, Y.; McKay, J. L.; Middlestead, P.; Ninnemann, U.; Nothaft, D.; Dubinina, E. O.; Quay, P.; Reverdin, G.; Shirai, K.; Mørkved, P. T.; Theiling, B. P.; Geldern, R. van; Wallace, D. W. R. An International Intercomparison of Stable Carbon Isotope Composition Measurements of Dissolved Inorganic Carbon in Seawater. *Limnol. Oceanogr.: Methods* **2019**, *17* (3), 200–209. https://doi.org/10.1002/lom3.10300.

(38) Sharp, J. H.; Cifuentes, L. A.; Coffin, R. B.; Pennock, J. R.; Wong, K.-C. The Influence of River Variability on the Circulation, Chemistry, and Microbiology of the Delaware Estuary. *Estuaries* **1986**, *9*, 261–269. https://doi.org/10.2307/1352098.

(39) Joesoef, A.; Kirchman, D. L.; Sommerfield, C. K.; Cai, W.-J. Seasonal Variability of the Inorganic Carbon System in a Large Coastal Plain Estuary. *Biogeosciences* **2017**, *14* (21), 4949–4963. https://doi.org/10.5194/bg-14-4949-2017.

(40) Joesoef, A.; Huang, W.-J.; Gao, Y.; Cai, W.-J. Air–Water Fluxes and Sources of Carbon Dioxide in the Delaware Estuary: Spatial and Seasonal Variability. *Biogeosciences* **2015**, *12* (20), 6085–6101. https://doi.org/10.5194/bg-12-6085-2015.

(41) Sharp, J. H. The Delaware Estuary: Research as Background for Estuarine Management and Development. *University of Delaware Sea Grant College Program*,**1984**.

(42) Yang, X.; Xue, L.; Li, Y.; Han, P.; Liu, X.; Zhang, L.; Cai, W.-J. Treated Wastewater Changes the Export of Dissolved Inorganic Carbon and Its Isotopic Composition and Leads to Acidification in Coastal Oceans. *Environ. Sci. Technol.* **2018**, *52* (10), 5590–5599. https://doi.org/10.1021/acs.est.8b00273.

(43) Jiang, L.-Q.; Cai, W.-J.; Wang, Y. A Comparative Study of Carbon Dioxide Degassing in River- and Marine-Dominated Estuaries. *Limnol. Oceanogr.* **2008**, *53* (6), 2603–2615. https://doi.org/10.4319/lo.2008.53.6.2603.

(44) Cotovicz, L. C.; Knoppers, B. A.; Deirmendjian, L.; Abril, G. Sources and Sinks of Dissolved Inorganic Carbon in an Urban Tropical Coastal Bay Revealed by δ^{13}C-DIC Signals. *Estuarine, Coastal Shelf Sci.* **2019**, *220*, 185–195. https://doi.org/10.1016/j.ecss.2019.02.048.

(45) Burdige, D. J.; Zimmerman, R. C.; Hu, X. Rates of Carbonate Dissolution in Permeable Sediments Estimated from Pore-Water Profiles: The Role of Sea Grasses. *Limnol. Oceanogr.* **2008**, 53 (2), 549–565. https://doi.org/10.4319/lo.2008.53.2.0549.

(46) Powell, E. N.; Kreeger, D. A.; Morson, J. M.; Haidvogel, D. B.; Wang, Z.; Thomas, R.; Gius, J. E. Oyster Food Supply in Delaware Bay: Estimation from a Hydrodynamic Model and Interaction with the Oyster Population. *J. Mar. Res.* **2012**, *70* (2–3), 469–503. https://doi.org/10.1357/002224012802851904.

(47) Mook, W. G. Environmental Isotopes in the Hydrological Cycle. Principles and Applications; UNESCO: Paris, **2001**.